Irregular excitation patterns in reaction-diffusion systems due to perturbation by secondary pacemakers

Claudia Lenk,[1,*] Mario Einax,[2,†] and Philipp Maass[2,‡]

[1]*Institut für Chemie und Biotechnik, Technische Universität Ilmenau, 98684 Ilmenau, Germany*

[2] *Fachbereich Physik, Universität Osnabrück, Barbarastraße 7, 49076 Osnabrück, Germany*

Spatiotemporal excitation patterns in the FitzHugh-Nagumo model are studied, which result from the disturbance of a primary pacemaker by a secondary pacemaker. The primary and secondary pacemakers generate regular waves with frequencies $f_{\rm pace}$ and $f_{\rm pert}$, respectively. The pacemakers are spatially separated, but waves emanating from them encounter each other via a small bridge. This leads to three different types I–III of irregular excitation patterns in disjunct domains of the $f_{\rm pace}$-$f_{\rm pert}$ plane. Types I and II are caused by detachments of waves coming from the two pacemakers at corners of the bridge. Type III irregularities are confined to a boundary region of the system and originate from a partial penetration of the primary waves into a space, where circular wave fronts from the secondary pacemaker prevail. For this type, local frequencies can significantly exceed $f_{\rm pace}$ and $f_{\rm pert}$. The degree of irregularity found for the three different types is quantified by the entropy of the local frequency distribution and an order parameter for phase coherence.

I. INTRODUCTION

Reaction-diffusion models are widely used to study the self-excitatory dynamics in different research fields. Prominent examples are the Bhelousov-Zhabotinsky reaction [1,2] and the catalysis of carbon monoxide [3,4] in chemistry, population [5] and plankton dynamics [6] as well as aggregation processes [7] in biology, and spreading of forest fires [8] in ecology. In physiology, reaction-diffusion models can be applied to study the propagation of electrical excitations in the brain [9] or heart [10]. Irregular excitation patterns in these systems, manifesting themselves in a spread of local activation frequencies, can result from a reduced or modified functionality of pathological states. Different causes for the appearance of these irregularities have been discussed in the literature, including nonlocal feedback [11,12], global changes of system properties such as excitability [13] and excitation thresholds [14], gradients in system parameters [15], changes due to remodeling [16,17] or mutations [18], influences of boundaries [19] or externally applied amplitude modulations [20], and the coupling between mechanical and electrical activation of the heart cells [21,22].

In this work we investigate another possible mechanism for the emergence of irregular excitation patterns, which is the perturbation of an initially regular activation by a secondary source. This mechanism can be important, for example, to understand electrophysiological observations during atrial fibrillation. Peculiar spatiotemporal patterns of the electric potential such as spiral waves, mother waves, or ectopic foci are thought to be responsible for this arrhythmia [10,23–26]. These patterns are often located near physiologically modified regions of the heart tissue in the left atrium [26–29], while the irregular fibrillatory states are often observed in the right atrium [28–30]. It is therefore important to better understand

how self-excitatory sources such as spiral waves or ectopic foci with rather regular dynamics in one region can induce irregular excitation patterns in another region.

Inspired by the idea that the mutual interference of originally regular wave fronts could be a cause of atrial fibrillation, we consider an idealized geometry where two pacemakers generate regular waves in two different areas that are connected by a small bridge. The primary pacemaker is thought to represent the sinus node in the right atrium, while the second pacemaker represents a self-excitatory source in the left atrium. To explore effects caused by the disturbance of the secondary pacemaker, we use the FitzHugh-Nagumo (FHN) model as one of the most studied standard reaction-diffusion systems for excitable media. Different types of irregularities are found in the area of the primary pacemaker and quantified by their phase coherence and the entropy of the local frequency distribution. With respect to the spatiotemporal dynamics of the electric potential in the atria, the FHN equations are certainly not realistic, but we are interested here in generic features, which may be independent of details such as the correct functional forms and duration of action potentials and the lengths of total and partial refractory periods.

II. MODEL

The FHN equations [31] are a set of two coupled nonlinear ordinary differential equations that describe excitable media via an inhibitor-activator mechanism. They were originally developed by searching for a simplified version of the Hodgkin-Huxley equations for electric pulse propagation along nerves [32]. When combined with a spatial diffusion term, the equations are

$$\frac{\partial u}{\partial t} = D\left(\frac{\partial^2 u}{\partial x^2} + \frac{\partial^2 u}{\partial y^2}\right) + c\left(v + u - \frac{u^3}{3} + z\right),$$
$$\frac{\partial v}{\partial t} = -\frac{1}{c}(u - a + bv). \tag{1}$$

*claudia.lenk@tu-ilmenau.de

†mario.einax@uni-osnabrueck.de

‡philipp.maass@uni-osnabrueck.de

The variable u is the fast activation variable, which describes the excitation of the system. The variable v is the inhibiting variable, which is responsible for driving the system back into the resting state after an excitation. The diffusion coefficient D describes a spatial coupling and z is an applied stimulus. The influence of the parameters a, b, and c can be inferred by numerical solutions of Eqs. (1) without the diffusive term. The parameter values are limited to some range, with respect to the ability to generate excitability, and their detailed effect on the pulses is complicated due to mutual interdependences originating from the nonlinearity in Eq. (1). Roughly speaking, a affects the length of the refractory period [33], b influences the stability of the resting state, and c controls the excitability and strength of the response to a stimulus. In the following we will associate the following set of parameters with the normal state of the system: $D = D_0 = 0.1$, $a = a_0 = 0.7$, $b = b_0 = 0.6$, and $c = c_0 = 5.5$. The resting state for this parameter set is given by the pair of values $u = u_0 = 1.2$ and $v = v_0 = -0.6$.

The two nonlinear coupled partial differential Eq. (1) are solved with the finite-element method, using a triangulation consisting of about 9000 nodes and an integration time step $\Delta t = 0.01$ [34]. Simulations with 130 000 nodes and time step $\Delta t = 0.005$ were performed to check the spatial and temporal resolution. The nonlinearity $u^3(\vec{x},t)$ in Eq. (1) is treated as an inhomogeneity, which means that for $u(\vec{x},t_i)$ the value $u(\vec{x},t_{i-1})$ of the preceding time step is used.

Calculations are carried out on a two-dimensional simulation area as shown in Fig. 1, which is considered to represent an isolated section of atrial heart tissue, as it is used often in experiments [35–37]. The simulation area has size 21×10 and is divided into three regions: the rectangular area L with $0 \leqslant x \leqslant 10$ and $0 \leqslant y \leqslant 10$ (representing the left atrium), the rectangular area R with $11 \leqslant x \leqslant 21$ and $0 \leqslant y \leqslant 10$ (representing the right atrium), and the small bridge B with $10 < x < 11$ and $4 < y < 6$ (representing fast conducting pathways between the electrically isolated atria
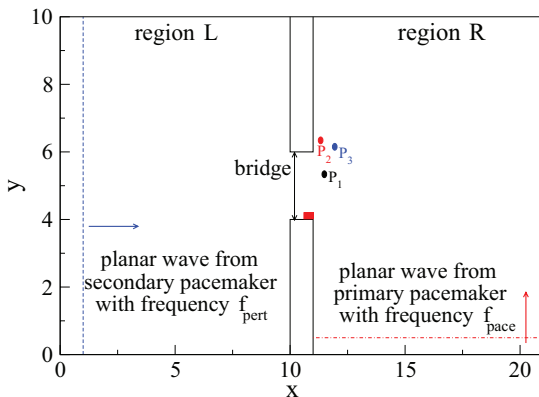

FIG. 1. (Color online) Sketch of the simulation area. In region R the primary pacemaker excites planar waves (red dash-dotted line) propagating in the y direction with frequency f_{pace}. In region L the secondary pacemaker generates planar waves (blue dashed line) propagating in the x direction with frequency f_{pert}. Here P_1, P_2, and P_3 mark the points for which time series of u are shown in Fig. 2. The red solid rectangle in the bridge ($10 < x < 11$ and $4 < y < 6$) indicates the region of detachment referred to in Sec. III.

such as Bachmann's bundle [38]). The boundaries conditions are of von Neumann type.

We focus on situations where the secondary pacemaker in region L is located far outside the left part of the simulation area, which allows us to treat the wave fronts as effectively planar [39]. In the simulations these secondary waves are generated by periodically applying a current $z = -1$ with duration one and period $1/f_{\text{pert}}$ in the region $x \leqslant 0.5$ and $0 \leqslant y \leqslant 10$. The primary waves representing the pacemaker in region R are generated analogously by periodically applying a current $z = -1$ with duration one and period $1/f_{\text{pace}}$ in the region $11 \leqslant x \leqslant 21$ and $y \leqslant 0.5$.

To quantify the irregularity (or, conversely, the regularity) of excitation patterns in region R we use two different methods. In the first method the Shannon entropy of the distribution of irregular frequencies is determined in region R. For every point on a grid with resolution $\Delta x = \Delta y = 0.1$, corresponding to a number $N_g = 100 \times 100$ of grid points, a local frequency is calculated as the inverse mean time interval between consecutive action potentials. To determine the frequency distribution, we divide the frequency range into N_b bins of size $\Delta f = 0.01$ and calculate the probabilities p_l of finding a frequency f in each bin $f_l \leqslant f \leqslant f_l + \Delta f$. The bins containing the pacing and perturbation frequencies are excluded from this analysis, i.e., only the irregular frequencies resulting from the interplay of the primary and secondary waves are considered. The (normalized) Shannon entropy of the irregular frequency distribution is

$$S(f_{\text{pace}}, f_{\text{pert}}) = -\frac{\sum_{l=1}^{N_b} p_l \ln p_l}{\ln N_b}. \tag{2}$$

For a single irregular frequency ($p_l = \delta_{l,l_0}$), $S = 0$, while for a chaotic pattern with a uniform frequency distribution ($p_l = 1/N_b$), $S = 1$. Notice that the local frequency distribution will depend sensitively on the pacemaker frequencies f_{pace} and f_{pert}, which we indicated by defining S as a function of these two frequencies in Eq. (2).

The second method quantifies the regularity by an order parameter Φ [40] for phase coherence in the system. To each potential $u_j(t)$ in element j of the grid, an imaginary part $\tilde{u}_j(t)$ is assigned by a Hilbert transform [41,42]

$$\tilde{u}_j(t) = \text{P.V.} \int \frac{dt'}{\pi} \frac{u_j(t')}{t - t'}, \tag{3}$$

where P.V. denotes Cauchy's principal value. Numerically, the Hilbert transform is carried out by a fast Fourier transform of $u_j(t)$, multiplication of the spectral components with $-i\,\text{sgn}(f)$ at frequency f, and Fourier back-transform into the time domain. With $\tilde{u}_j(t)$ known, a phase $\varphi_j(t) = \arctan[\tilde{u}_j(t)/u_j(t)]$ can be associated with the signal at time t in each element j. The order parameter for phase coherence is defined by

$$\Phi(f_{\text{pace}}, f_{\text{pert}}) = \frac{2}{N_g(N_g - 1)} \sum_{j>k}^{N_g} |\langle \exp\{i[\varphi_j(t) - \varphi_k(t)]\}\rangle_t|, \tag{4}$$

where $\langle \cdots \rangle_t$ denotes a time average. In practice, we have taken a moving average $\langle \cdots \rangle_t = T^{-1} \int_{t_0}^{t_0+T} dt \cdots$ in a time

interval $T \gg \max(f_{\text{pace}}^{-1}, f_{\text{pert}}^{-1})$ and checked that $\Phi(f_{\text{pace}}, f_{\text{pert}})$ fluctuates around a constant value after evolving the system into a stationary state.

III. INFLUENCE OF SECONDARY PACEMAKER ON PRIMARY WAVES

The secondary pacemaker can be expected to have a destabilizing effect on an *a priori* regular propagation of the primary waves. In certain circumstances it is also conceivable that a stabilization of an irregular excitation pattern of the primary waves occurs. The formation of irregularities by the secondary pacemaker is demonstrated in Fig. 2, where the time evolution of u is shown at the three points P_i marked in Fig. 1 for $f_{\text{pace}} = 0.091$ and $f_{\text{pert}} = 0.1$ and 0.105. While for $f_{\text{pert}} = 0.1$ [Fig. 2(a)] the evolution remains regular, irregular behavior is found for the slightly higher frequency $f_{\text{pert}} = 0.105$ [Fig. 2(b)]. This is reflected in changes of the shape of the action potential $u(t)$ [see, for example, the unsuccessful activation at point P_2 (dashed line) at $t = 175$].

Spatial irregularity expresses itself by wave breaks, wave fragments, or instabilities with reentrant characteristics and examples of it will be shown in the following section. With respect to the formation of irregularities in region R, we can distinguish three different regimes I–III in the f_{pace}-f_{pert} plane (see Fig. 3). The decisive quantity separating these domains is the critical frequency f_c [43,44], above which traveling planar waves detach from sharp corners. We determined this critical frequency by evaluating the velocity $\tilde{v}_x$ of the primary wave (region R) in the x direction at the lower left corner ($x \simeq 10.9$ and $y \simeq 4.1$) of the bridge when the secondary pacemaker is absent ($f_{\text{pert}} = 0$). The velocity is calculated by tracking the peak position of the action potential. For small pacing frequencies the velocity $\tilde{v}_x$ is negative where its magnitude
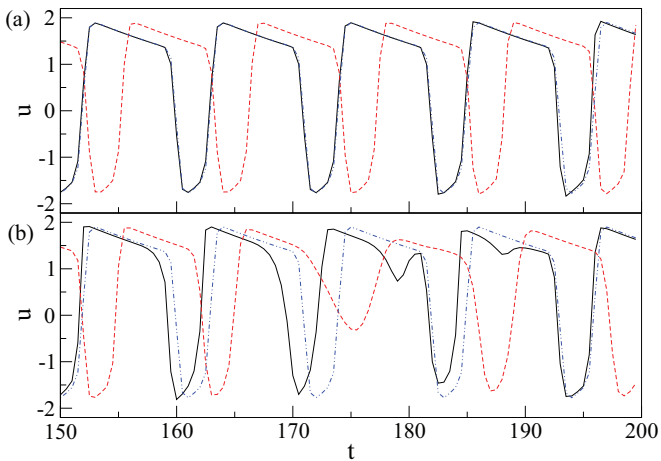

FIG. 2. (Color online) Time evolution of the activation variable u at three points marked in Fig. 1, $P_1 = (11.49, 5.34)$ (black solid line), $P_2 = (11.33, 6.34)$ (red dashed line), and $P_3 = (11.94, 6.15)$ (blue dash-dotted line), for a pacing frequency $f_{\text{pace}} = 0.091$ and two different perturbation frequencies (a) $f_{\text{pert}} = 0.1$ and (b) $f_{\text{pert}} = 0.105$. It was checked that the behavior remains qualitatively the same after a three times longer simulation time, which gives confidence that the obtained features are not a transient phenomenon.
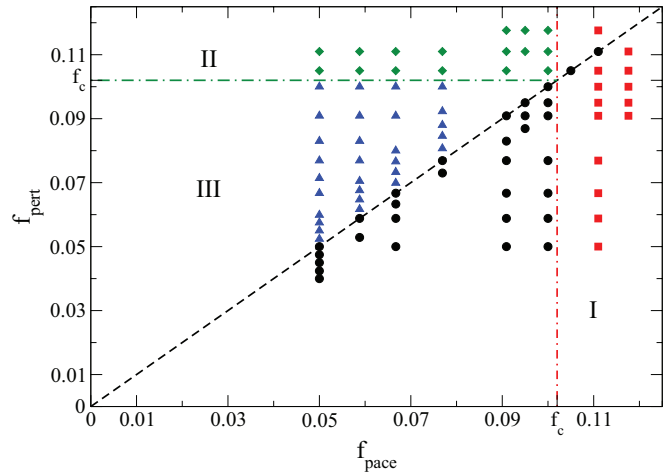

FIG. 3. (Color online) The three domains in the f_{pace}-f_{pert} plane, where different types of irregularities occur. The symbols mark the points where solutions of the FHN equations (1) have been generated. Circles refer to solutions where regular excitation patterns have been obtained and squares, diamonds, and triangles refer to solutions where irregularities of types I, II, and III, respectively have been found. The scale of the frequencies is limited to $f = 0.1176$. Above this frequency planar waves cannot be excited if the frequency of generated wave fronts corresponds to the pacing frequency in a one-to-one manner.

becomes smaller with increasing f until reaching zero at $f = f_c$. For our parameters (see Sec. II) we find $f_c = 0.102$.

While the phenomenon of detachment from sharp corners is known both theoretically [43–45] and experimentally [44,45], the question of how this primary effect affects the excitation patterns arising from colliding waves of the two pacemakers has not been established yet. In the following we discuss spatiotemporal excitation patterns in the three regimes I–III and characterize them with respect to (i) the ratio of the highest local frequency $f_{\text{max}} = \max_l f_l$ found in region R to the pacing frequency, (ii) the entropy S in Eq. (2), and (iii) the phase coherence of the resulting patterns, described by the order parameter Φ.

A. Spatiotemporal excitation patterns in regimes I–III

Regime I corresponds to high pacing frequencies $f_{\text{pace}} > f_c$ (see Fig. 3), where the primary planar waves detach from the lower corner of the bridge. Planar wave fronts with open ends curl in the direction opposite to the propagation direction of the front. In the absence of secondary waves, this leads to the known irregularities initiated by such curling. In the presence of perturbing secondary wave fronts, it is however conceivable that the detachment of the primary waves is effectively avoided.

A typical situation for the possible occurrence of this effect and its further time evolution is followed in Fig. 4. Figure 4(a) refers to a time instant where one of the primary waves approaches the lower corner of the bridge and a detached wave with an open end is propagating ahead of it. With progressing time the primary wave transverses the bridge while merging with a secondary wave that passes through the bridge at the same time [Figs. 4(b) and 4(c)]. As a consequence, the merged
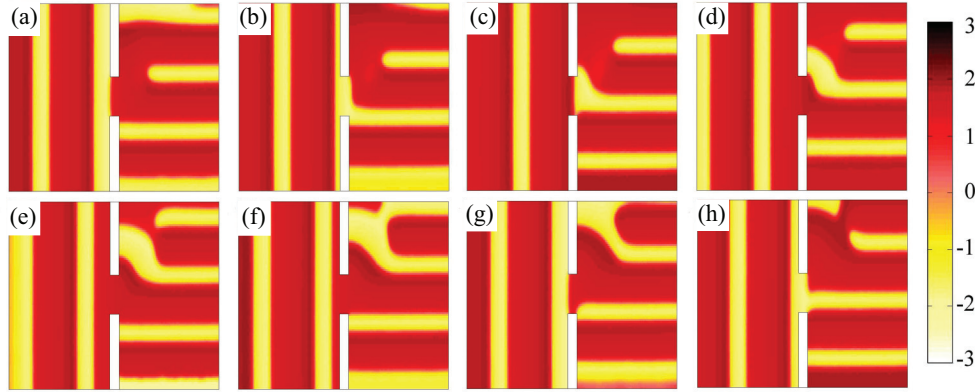
FIG. 4. (Color online) Time evolution of u for irregularity type I for $f_{\text{pace}} = 0.117$ and $f_{\text{pert}} = 0.091$. Time steps between the pictures are (a)–(e) $\Delta t = 4$ and (f)–(h) $\Delta t = 3$. The color coding is given by the bar on the right. Yellow refers to the excited state and red to the excitable or refractory state.

wave front is not detached from the boundary after the bridge has been transversed [see Fig. 4(d)]. The secondary wave thus leads to a pattern where an open end of a wave front is first avoided. However, the curling of the wave with an open end running ahead [Fig. 4(e)] leads to a merger with the wave still having contact with the boundary. As a result, a fork-type shape of the excited area in the upper part of region R is seen in Fig. 4(f). Because the part connecting the lower tooth with the stem cannot propagate into the refractory area between the teeth, this part becomes thinner [Fig. 4(g)] and eventually a rupture of the excitation front takes place [Fig. 4(h)]. Hence, despite the initial avoidance of a detachment after traversal of the bridge, eventually a wave front with an open end again results.

For $f_{\text{pace}} < f_c$, the primary waves, in the absence of the second pacemaker, would exhibit planar wave fronts with contact with the boundaries, propagating regularly in the y direction. The question is whether this regularity is destroyed by the secondary pacemaker.

In regime II $f_{\text{pert}} > f_c$ (and $f_{\text{pace}} < f_c$) (see Fig. 3), the secondary waves detach from the corners of the bridge, leading to two open ends of the wave fronts after passing the bridge.

These open ends start to curl, which in the absence of the primary waves can lead to two counterrotating spirals. In the case of an interplay of the propagating open ends with the primary waves, complex excitation patterns emerge in region R. An additional source of this complexity is that due to the high f_{pert}, the time periods of excitability in the region R near the bridge are rather short and accordingly the propagation of the primary waves cannot be continued in this area, i.e., detachment of the primary waves takes place close to the bridge.

An example of the spatiotemporal behavior in regime II is shown in Fig. 5. In Fig. 5(a) two subsequent fronts of the primary waves in region R can be seen, where the front running ahead has detached from the boundary and the left open end is already curled. A secondary wave has just passed the bridge and exhibits two open ends. In the course of time, the curled primary wave front merges with the secondary wave front [Figs. 5(b) and 5(c)]. Subsequently, a further merger with the following primary wave occurs, resulting in a pattern where the two primary wave fronts are connected by a thin stripe parallel to the y axis [Fig. 5(d)]. The lower part of this stripe can propagate in the x direction, while a corresponding
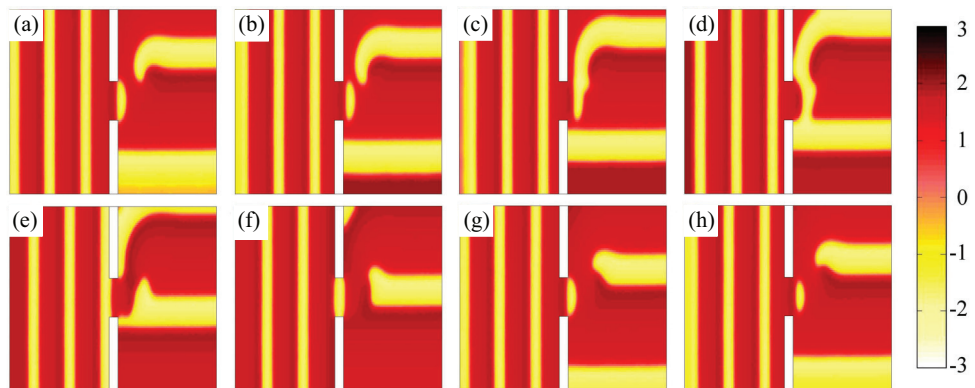

FIG. 5. (Color online) Time evolution of u for irregularity type II for $f_{\text{pace}} = 0.091$ and $f_{\text{pert}} = 0.105$. Time steps between the pictures are (a)–(d) $\Delta t = 2$ and (e)–(h) $\Delta t = 4$. The color coding is given by the bar on the right. Yellow refers to the excited state and red to the excitable or refractory state.

FIG. 6. (Color online) Time evolution of u for irregularity type III for $f_{pace} = 0.067$ and $f_{pert} = 0.100$. Time steps between the pictures are (a)–(d) $\Delta t = 2$ and (e)–(h) $\Delta t = 4$. The color coding is given by the bar on the right. Yellow refers to the excited state and red to the excitable or refractory state.
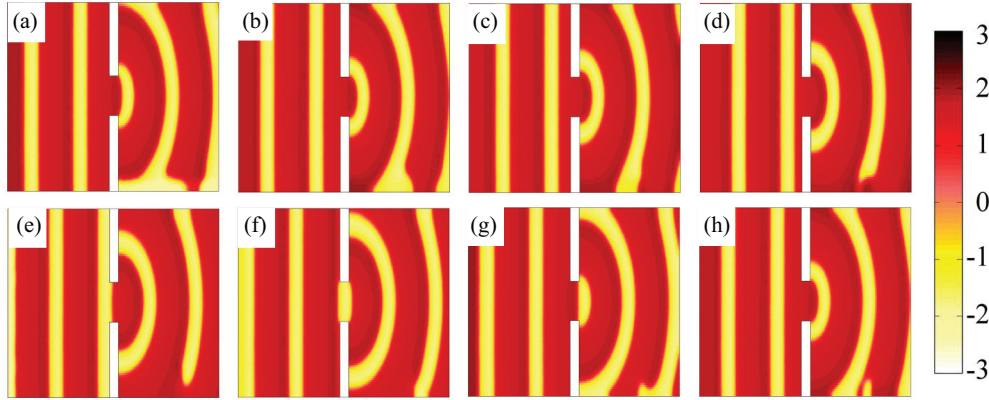
propagation of the upper part is hindered because the primary wave running ahead has left behind a refractory area. As a result, the stripe ruptures [Fig. 5(e)]. At the same time the following primary wave cannot enter the area in front of the bridge due to the missing excitability discussed above. With further time this wave is detached from the boundary [Fig. 5(f)], another secondary wave passes through the bridge [Fig. 5(g)], and eventually an excitation pattern [Fig. 5(h)] corresponding to a situation shortly before the pattern in Fig. 5(a) is obtained.

In regime III, $f_{pert} > f_{pace}$ and both f_{pert} and f_{pace} are smaller than f_c. After passing the bridge the secondary waves now keep contact with the boundary and form circular wave fronts that spread out in region R. Because $f_{pert} > f_{pace}$ these circular waves expel the primary waves after a transient time. A representative example of the spatial activation pattern and its temporal evolution is shown in Fig. 6. Overall the circular waves represent a regular pattern. However, the primary waves activated at the lower boundary in region R can partially penetrate the space between the circular wave fronts and thus build up wave fragments [see Figs. 6(a), 6(b), 6(g), and 6(h)]. Irregularities in regime III are thus confined to a boundary layer.

Since the irregular features occur in small domains that are located near the bridge for type I and II irregularity and near the lower right boundary for type III irregularity, one should expect them to be essentially unaffected by the system size. Indeed, by carrying out additional calculations for a larger system, where we extended the right region R from $11 < x < 21$ and $0 < y < 10$ to $11 < x < 31$ and $0 < y < 20$, we recovered all three types of irregularities in the extended system.

B. Strength of irregularities in regimes I–III

Figure 7 shows the maximal local frequency f_{max} as a function of f_{pert} for five different pacing frequencies f_{pace}. As long as $f_{pert} \leqslant f_{pace}$, the activation patterns are regular and $f_{max} = f_{pace}$. If $f_{pace} < f_c = 0.102$ (all curves except the one marked by the green triangles), regime III is first entered when f_{pert} becomes larger than f_{pace} (see Fig. 3). The irregularities in this regime are reflected by f_{max} values that in general

exceed f_{pert} slightly. In certain cases the enhancement can be quite large, as evidenced by the value $f_{max} \simeq 0.15$ found for $f_{pace} = 0.05$ (black circles) at $f_{pert} = 0.1$. For $f_{pert} > f_c$, regime II is entered (right of dotted line in Fig. 7). In this regime f_{max} is weakly enhanced with respect to f_{pert}. In the situation where $f_{pace} > f_c$ (curve marked by the green triangles), which corresponds to regime I (see Fig. 3), a similar moderate enhancement of f_{max} with respect to f_{pace} is obtained.

The entropy S and the order parameter Φ of phase coherence [see Eq. (2)] are displayed in Fig. 8 as a function of f_{pert} for the same set of fixed pacing frequencies as in Fig. 7. Figures 8(a) (for S) and 8(c) (for Φ) refer to the area $y < 4$ below the lower corner of the bridge (see Fig. 1), while Figs. 8(b) (for Φ) and 8(d) (for S) refer to $y > 4$, where the corner detachments of the waves can have an influence. With both measures changes in the degree of regularity of the excitation patterns can be clearly identified. Transitions
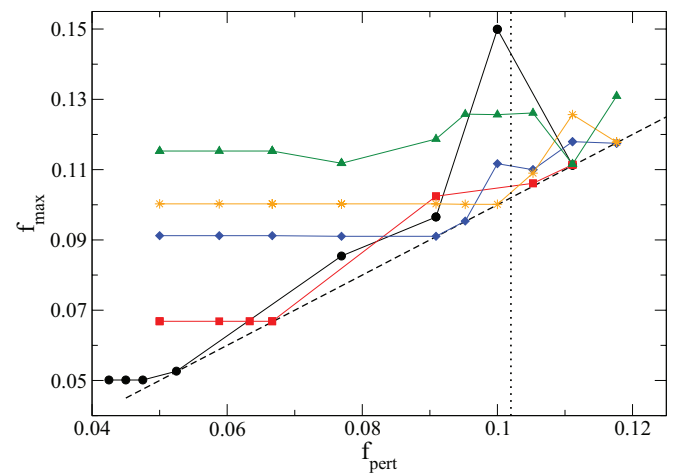

FIG. 7. (Color online) Maximal local frequency in region R as a function of f_{pert} for different pacing frequencies $f_{pace} = 0.050$ (black circles), 0.067 (red squares), 0.091 (blue diamonds), 0.10 (orange stars), and 0.111 (green triangles). The dotted line marks the critical frequency f_c and the case $f_{max} = f_{pert}$ is indicated by the dashed line. The solid lines connecting the data points are drawn as a guide for the eye.
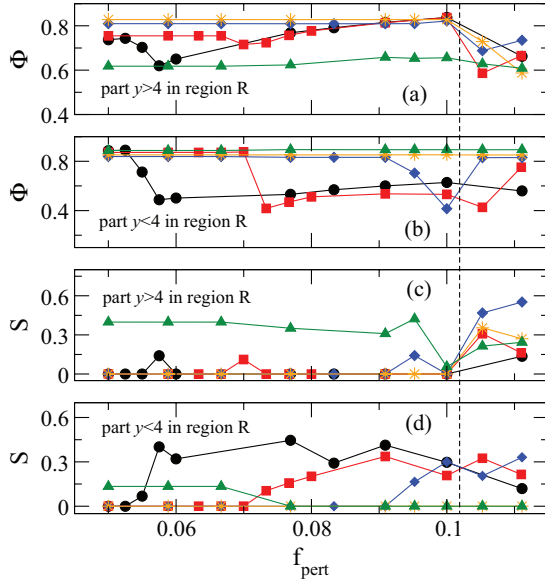
FIG. 8. (Color online) Order parameter Φ for phase coherence and entropy S of the local frequency distribution dependent on the perturbation frequency f_{pert}, calculated for areas (a) and (c) $y > 4$ and (b) and (d) $y < 4$ in region R. Results are shown for different pacing frequencies: $f_{\text{pace}} = 0.050$ (black circles), 0.067 (red squares), 0.091 (blue diamonds), 0.10 (orange stars), and 0.111 (green triangles). The vertical dashed line marks the critical frequency f_c.

from more regular to less regular states are reflected in decreases of Φ and increases of S, respectively. Focusing on the behavior of Φ, the transition from the regular regime to regime III is seen in Fig. 8(b) as a sharp drop after which Φ remains essentially constant upon further increasing f_{pert} below f_c (left of the dotted line). In Fig. 8(a) the drop of Φ becomes less pronounced with increasing f_{pace} and is followed by a smooth increase. This can be understood from the fact that the irregularity in regime III is confined to the lower boundary of region R. With increasing f_{pert} the regularity induced by the secondary waves in the upper part of region R can be more easily established and the perturbations induced by the irregularities at the lower boundary become less relevant. In the lower part of region R by contrast, the effects induced by the irregularities at the lower boundary prevail and accordingly Φ is not significantly affected by f_{pert}. The transition from regime III to II is reflected in a drop of Φ in Fig. 8(a). In Fig. 8(b) the behavior is more complicated. For small f_{pace} (curves marked by black circles and red squares) the irregularities in the upper part of region R can penetrate to the lower part and accordingly Φ is small. In fact, the Φ values are comparable to the ones obtained for $f_{\text{pert}} < f_c$. As a consequence, the transition from regime III to II cannot be seen clearly in the data. For larger f_{pace} (curve marked by blue diamonds) the penetration of the irregularities from the upper to the lower part of region R is suppressed, which is reflected in an increase of Φ when f_{pert} exceeds f_c. For $f_{\text{pace}} > f_c$ (curve marked by green triangles), where the system stays in regime I, a small constant Φ value is obtained in Fig. 8(a) and a large constant value in Fig. 8(b) as a result of the detachment of the primary waves at the bridge.

While both measures S and Φ are well suited to identify transitions between different regimes of irregularity, they can show different behavior in detail. The entropy S quantifies the spread in local frequencies, while the order parameter Φ is more sensitive to correlations in the spatiotemporal behavior. For example, in the case $f_{\text{pace}} > f_c$ (curve marked by green triangles) the entropy in the upper part of region R [Fig. 8(c)] shows some variations when f_{pert} is close to f_c in contrast to Φ [Fig. 8(a)]. In contrast, the slow rise of Φ for small pacing frequencies after entering regime III [curves marked by black circles and red squares in Fig. 8(a); see discussion above] is not seen in S [Fig. 8(c)].

It is interesting that the highest local frequencies are obtained in regime III, where neither the primary nor the secondary waves detach from the bridge. In contrast, one has to keep in mind that the irregularities at the boundaries leading to these high frequencies appear after some transient time t_{tr}, which depends on f_{pert} and f_{pace}. To quantify this effect we define t_{tr} by the time where the order parameter starts to deviate significantly from its value in the unperturbed system [46]. As shown in Fig. 9, t_{tr} decreases with f_{pert} (at fixed f_{pace}) and increases with f_{pace} (at fixed f_{pert}). This can be intuitively understood from the fact that the penetration of the secondary waves in the region R should occur faster the larger the difference $f_{\text{pert}} - f_{\text{pace}}$ is. When f_{pert} is approaching f_{pace}, t_{tr} appears to diverge.

In fact, for large t_{tr}, the functional dependence on f_{pert} and f_{pace} can be determined by considering that the secondary waves have to reach the lower boundary in region R and on their way the leading penetrating front is effectively annihilated once it collides with a front of the primary waves. This effective annihilation is caused by the refractory area following the front of the primary wave. In the time interval between two annihilations, the leading front of the secondary travels a distance $\Delta s' = (v/f_{\text{pace}} + v/f_{\text{pert}})/2$, where v is the
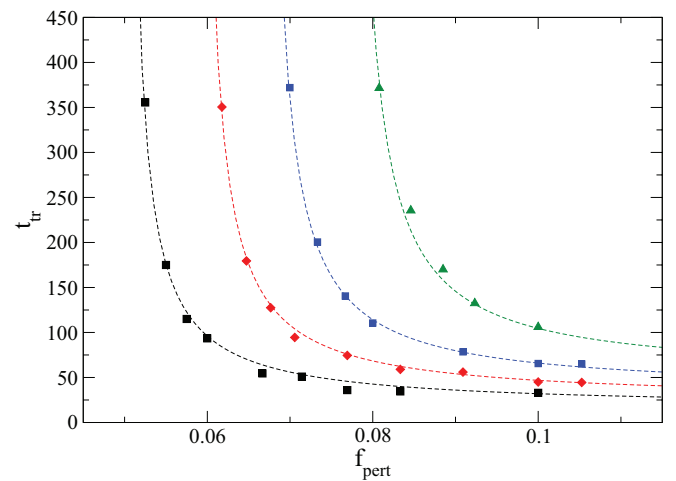

FIG. 9. (Color online) Transient time t_{tr} before onset of irregularities in regime III as a function of f_{pert} for $f_{\text{pace}} = 0.050$ (black circles), 0.059 (red diamonds), 0.067 (blue squares), and 0.077 (green triangles). Dashed lines are calculated according to Eq. (5) with $t_a = 0$ for $f_{\text{pace}} = 0.05$ (black line), $t_a = 9$ for $f_{\text{pace}} = 0.0588$ (red line), $t_a = 18$ for $f_{\text{pace}} = 0.0667$ (blue line), and $t_a = 36$ for $f_{\text{pace}} = 0.077$ (green line).

velocity of wave propagation ($v \simeq 1$ in our units for the chosen parameters). After this time, the leading front is annihilated and the following one is propagating until it is also annihilated. Because the distance between two subsequent fronts of the secondary wave is v/f_{pert}, the distance between two successive annihilated fronts (i.e., the increment in the penetration depth) is $\Delta s = \Delta s' - v/f_{pert}$. Let us denote by s_0 the travel distance of the secondary wave to the lower boundary of region R after the first annihilation, i.e., the size of the penetration area. A number $n = s_0/\Delta s$ of annihilations then occurs before the secondary wave reaches the lower boundary in region R. Accordingly, for large transient times ($f_{pert} \searrow f_{pace}$) we obtain $t_{tr} \sim n/f_{pace} = 2s_0 f_{pert}/[v(f_{pert} - f_{pace})]$. For small transient times, the accommodation of the action potential duration and propagation velocity to excitation frequency gives a non-negligible contribution, which can be effectively taken into account by an additive time t_a. This leads to

$$t_{tr} \simeq \frac{2s_0}{v} \frac{f_{pert}}{f_{pert} - f_{pace}} + t_a. \qquad (5)$$

In our setting where the first primary and first secondary waves are generated at the same time instant, $s_0 = 16/2 = 8$ (see Fig. 1). As shown by the dashed lines in Fig. 9, this equation describes well the simulated data.

IV. CONCLUSION

The appearance of self-excitatory sources as ectopic foci or spiral waves is widely assumed to be a condition for the emergence of irregular excitation patterns, although these sources can generate quite regular excitations. In this context it can be conjectured that irregularities emerge from the interaction of waves from two different sources, for example, waves of an ectopic focus collide with waves originating from a pacemaker. In previous studies on interactions of paced with self-excitatory waves, the influence of pacing on a spiral wave was studied, e.g., by Osipov *et al.* [47] and Davidenko *et al.* [48] with the aim of suggesting a possible therapy to suppress fibrillation or tachycardia in the heart. The pacing was applied to the region where the spiral wave was located. It was found that it leads to an annihilation of the reentrant activity or to a shift of the spiral core [48–51].

This work studies the interaction of two pacemakers under geometrical constraints. In an idealized geometry, resembling a connection between the left and right atria in the heart, three different types of irregular excitation patterns could be identified. Which of these types occurs depends on the frequencies f_{pace} and f_{pert} of the two pacemakers. We showed that in addition to the entropy S of the local frequency distribution, the order parameter Φ for phase coherence is a useful measure for quantifying the degree of irregularity. Transitions between regular and irregular behavior and between different types of irregularities can be identified with both measures.

The type III irregularity yields local frequencies that can significantly exceed the pacing and perturbation frequencies. It might be a possible cause of atrial fibrillation, for example, when one considers L to represent the left atrium with a self-excitatory source and R the right atrium paced by the sinus node. With respect to the condition $f_{pert} > f_{pace}$ for type III irregularity to occur, it is interesting to note that the frequency of a self-excitatory pacemaker in the left atrium often has a higher frequency than the sinus node [28,29]. In the future it will be of particular interest to see whether this mechanism of generating irregular excitation patterns can be found in more realistic model equations for atrial electrophysiology, e.g., in the model of Courtemanche *et al.* [52] or that of Bueno-Orovio *et al.* [53]. Furthermore, the role of spatial inhomogeneities should be clarified with respect to the different mechanisms leading to the irregularities.

ACKNOWLEDGMENTS

[1] S. M. Tobias and E. Knobloch, Phys. Rev. Lett. **80**, 4811 (1998).

[2] M. Bär and M. Eiswirth, Phys. Rev. E **48**, R1635 (1993).

[3] S. Jakubith, H. H. Rotermund, W. Engel, A. von Oertzen, and G. Ertl, Phys. Rev. Lett. **65**, 3013 (1990).

[4] G. Ertl, Science **254**, 1750 (1991).

[5] M. G. Clerc, D. Escaff, and V. M. Kenkre, Phys. Rev. E **72**, 056217 (2005).

[6] L. S. Schulman and P. E. Seiden, Science **233**, 425 (1986).

[7] K. J. Lee, E. C. Cox, and R. E. Goldstein, Phys. Rev. Lett. **76**, 1174 (1996).

[8] V. Mendez and J. E. Llebot, Phys. Rev. E **56**, 6557 (1997).

[9] F. M. Schneider and E. Schöll, Chaos **19**, 015110 (2009).

[10] S. Nattel, Nature **415**, 219 (2002).

[11] E. M. Nicola, M. Bär, and H. Engel, Phys. Rev. E **73**, 066225 (2006).

[12] S. W. Morgan, G. Plank, I. V. Biktasheva, and V. N. Biktashev, Biophys. J. **96**, 1364 (2009).

[13] C. Luengviriya, U. Storb, G. Lindner, S. C. Müller, M. Bär, and M. J. B. Hauser, Phys. Rev. Lett. **100**, 148302 (2008).

[14] A. T. Winfree, Chaos **1**, 303 (1991).

[15] C. Qiao, Y. Wu, X. C. Lu, C. Y. Wang, Q. Ouyang, and H. Wang, Chaos **18**, 026109 (2008).

[16] S. Kharche, C. J. Garratt, M. R. Boyett, S. Inada, A. V. Holden, J. C. Hancoux, and H. Zhang, Prog. Biophys. Mol. Biol. **98**, 186 (2008).

[17] H. Zhang, C. J. Garratt, S. Kharche, and A. V. Holden, Physica D **238**, 976 (2009).

[18] G. Seemann, P. Carillo, D. L. Weiss, M. W. Krueger, O. Dössel, and E. P. Scholz, in *Proceedings of the International Conference on Functional Imaging and Modeling of the Heart, Nice, 2009*, edited by N. Ayache, H. Delingette, and M. Sermesant (Springer, Berlin, 2009), p. 144.

[19] M. D. Graham, M. Bär, I. G. Kevrekidis, K. Asakura, J. Lauterbach, H.-H. Rotermund, and G. Ertl, Phys. Rev. E **52**, 76 (1995).

[20] J. E. Pearson, Science **261**, 189 (1993).

[21] V. V. Yashin and A. Balazs, Science **314**, 798 (2006).

[22] A. V. Panfilov, R. H. Keldermann, and M. P. Nash, Proc. Natl. Acad. Sci. USA **104**, 7922 (2007).

[23] S. Nattel, D. Li, and L. Yue, Annu. Rev. Phys. **62**, 51 (2000).

[24] S. Nattel and L. H. Opie, Lancet **367**, 262 (2006).

[25] S.-A. Chen, M.-H. Hsieh, C.-T. Tai, C.-F. Tsai, V. S. Prakash, W.-C. Yu, T.-L. Hsu, Y.-A. Ding, and M.-S. Chang, Circulation **100**, 1879 (1999).

[26] R. Mandapati, A. Skanes, Y. Chen, O. Berenfeld, and J. Jalife, Circulation **101**, 194 (2000).

[27] T.-J. Wu, M. Yashima, F. Xie, C. A. Athill, Y.-H. Kim, M. C. Fishbein, Z. Qu, A. Garfinkel, J. N. Weiss, H. S. Karagueuzian, and P.-S. Chen, Circ. Res. **83**, 448 (1998).

[28] J. Sahadevan, K. Ryu, L. Peltz, C. M. Khrestian, R. W. Stewart, A. H. Markowitz, and A. L. Waldo, Circulation **110**, 3293 (2004).

[29] P. Sanders, O. Berenfeld, M. Hocini, P. Jais, R. Vaidyanathan, L.-F. Hsu, S. Garrigue, Y. Takahashi, M. Rotter, F. Sacher, C. Scavee, R. Ploutz-Snyder, J. Jalife, and M. Haisaguerre, Circulation **112**, 789 (2005).

[30] S. Lazar, S. Dixit, F. E. Marchlinski, D. J. Callans, and E. P. Gerstenfeld, Circulation **110**, 3181 (2004).

[31] R. FitzHugh, Biophys. J. **1**, 445 (1959).

[32] A. L. Hodgkin and A. F. Huxley, J. Physiol. **117**, 500 (1952).

[33] That is, the time interval during which the system cannot be excited again.

[34] One time unit corresponds to about 50 ms.

[35] T. Ikeda, M. Yashima, T. Uchida, D. Hough, and M. C. Fishbein, Circ. Res. **81**, 753 (1997).

[36] S. Iravanian, Y. Nabutovsky, C.-R. Kong, S. Saha, N. Bursac, and L. Tung, Am. J. Physiol. Heart Circ. Phys. **285**, H449 (2003).

[37] T. Ikeda, L. Czer, A. Trento, C. Hwang, J. J. C. Ong, D. Hough, M. C. Fishbein, W. J. Mandel, H. S. Karagueuzian, and P.-S. Chen, Circulation **96**, 3013 (1997).

[38] R. Lemery, L. Soucie, B. Martin, A. S. L. Tang, M. Green, and J. Healey, Circulation **110**, 2083 (2004).

[39] For wave propagation in two dimensions it would be more correct to speak about "line wave fronts," but since this term is not common, we use the term "planar wave fronts" in the following.

[40] A. F. Taylor, P. Kapetanopoulos, B. J. Whitaker, R. Toth, L. Bull, and M. R. Tinsley, Eur. Phys. J. Spec. Top. **165**, 137 (2008).

[41] D. Gabor, J. IEE (London) **93**, 429 (1946).

[42] B. Boashash, Proc. IEEE **80**, 520 (1992); **80**, 540 (1992).

[43] J. M. Starobin, Y. I. Zilberter, E. M. Rusnak, and C. F. Starmer, Biophys. J. **70**, 581 (1996).

[44] K. Agladze, J. P. Keener, S. C. Müller, and A. Panfilov, Science **164**, 1746 (1994).

[45] C. Cabo, A. M. Pertsov, J. M. Davidenko, and J. Jalife, Chaos **8**, 116 (1998).

[46] To be specific, we analyzed the time-dependent order parameter $\tilde{\Phi}(t, f_{\text{pace}}, f_{\text{pert}}) = \frac{2}{N_g(N_g-1)} \sum_{j>k}^{N_g} |\exp\{i[\varphi_j(t) - \varphi_k(t)]\}|$ and fixed t_{tr} by the time instant where it differs from the corresponding parameter $\tilde{\Phi}(t_{\text{tr}}, f_{\text{pace}}, f_{\text{pert}} = 0)$ in the unperturbed system by the amount 0.2, i.e., $|\tilde{\Phi}(t_{\text{tr}}, f_{\text{pace}}, f_{\text{pert}} = 0) - \tilde{\Phi}(t_{\text{tr}}, f_{\text{pace}}, f_{\text{pert}})| = 0.2$.

[47] G. V. Osipov, A. T. Stamp, and J. J. Collins, in *Proceedings of the Second International Conference on Control of Oscillations and Chaos, St. Petersburg, 2000*, edited by F. L. Chernousko and A. L. Fradkov (IEEE, Piscataway, NJ, 2000), Vol. 3, p. 453.

[48] J. M. Davidenko, R. Salomonsz, A. M. Pertsov, W. T. Baxter, and J. Jalife, Circ. Res. **77**, 1166 (1995).

[49] K. Agladze, M. W. Kay, V. Krinsky, and N. Savazyan, Am. J. Physiol. Heart Circ. Phys. **293**, H503 (2007).

[50] Y.-Q. Fu, H. Zhang, Z. Cao, B. Zheng, and G. Hu, Phys. Rev. E **72**, 046206 (2005).

[51] G. Gottwald, A. Pumir, and V. Krinsky, Chaos **11**, 487 (2001).

[52] M. Courtemanche, R. J. Ramirez, and S. Nattel, Am. J. Phys. **275**, H301 (1998).

[53] A. Bueno-Orovio, E. M. Cherry, and F. H. Fenton, J. Theor. Biol. **253**, 544 (2008).